J|A|C|S ARTICLES

Published on Web 08/02/2010

Quantum Chemical Modeling of Benzene Ethylation over H-ZSM-5 Approaching Chemical Accuracy: A Hybrid MP2:DFT Study

Niels Hansen,*,† Torsten Kerber,‡ Joachim Sauer,*,‡ Alexis T. Bell,§ and Frerich J. Keil†

Department of Chemical Engineering, Hamburg University of Technology, D-21073 Hamburg, Germany, Institut für Chemie, Humboldt-Universität zu Berlin, D-10099 Berlin, Germany, and Department of Chemical Engineering, University of California, Berkeley, California 94720-1462

Received March 17, 2010; E-mail: n.hansen@tuhh.de (N. Hansen); js@chemie.hu-berlin.de (J. Sauer)

Abstract: The alkylation of benzene by ethene over H-ZSM-5 is analyzed by means of a hybrid MP2:DFT scheme. Density functional calculations applying periodic boundary conditions (PBE functional) are combined with MP2 energy calculations on a series of cluster models of increasing size which allows extrapolation to the periodic MP2 limit. Basis set truncation errors are estimated by extrapolation of the MP2 energy to the complete basis set limit. Contributions from higher-order correlation effects are accounted for by CCSD(T) coupled cluster calculations. The sum of all contributions provides the "final estimates" for adsorption energies and energy barriers. Dispersion contributes significantly to the potential energy surface. As a result, the MP2:DFT potential energy profile is shifted downward compared to the PBE profile. More importantly, this shift is not the same for reactants and transition structures due to different self-interaction correction errors. The final enthalpies for ethene, benzene, and ethylbenzene adsorption on the Brønsted acid site at 298 K are −46, −78, and −110 kJ/mol, respectively. The intrinsic enthalpy barriers at 653 K are 117 and 119/94 kJ/mol for the one- and two-step alkylation, respectively. Intrinsic rate coefficients calculated by means of transition state theory are converted to apparent Arrhenius parameters by means of the multicomponent adsorption equilibrium. The simulated apparent activation energy (66 kJ/mol) agrees with experimental data (58−76 kJ/mol) within the uncertainty limit of the calculations. Adsorption energies obtained by adding a damped dispersion term to the PBE energies (PBE+D), agree within ±7 kJ/mol, with the "final estimates", except for physisorption (π-complex formation) and chemisorption of ethene (ethoxide formation) for which the PBE+D energies are 12.4 and 26.0 kJ/mol, respectively larger than the "final estimates". For intrinsic energy barriers, the PBE+D approach does not improve pure PBE results.

1. Introduction

Zeolites are used as catalysts in the petroleum and chemical industries to promote a large number of reactions.[1,2] For this reason considerable interest has been devoted in recent years toward the development of theoretical models for describing adsorption, diffusion, and reaction in zeolites and toward the clarification of how these processes are affected by zeolite structure and composition.[3,4] The ultimate aim of such work is to simulate the activity and selectivity of zeolite catalysts from first principles. An essential part of this ongoing effort is the development of accurate methods for the prediction of the energies of adsorption/desorption and reaction, as well as the rate coefficients for these processes.

Density functional theory (DFT) is now routinely applied to calculate the energy profiles of chemical reactions for systems as large as zeolites. However, the use of DFT is hampered by the fact that functionals which can be used efficiently in solid-state simulations do not properly account for long-range dispersion interactions[5,6] and are subject to the self-interaction error.[7,8] This results in underestimated adsorption energies[9,10] and energy barriers that are systematically too low,[11,12] respectively. For noncovalently bonded complexes and large molecules[13−15] as well as for solid-state and adsorption problems[10,16,17] it has been shown that the dispersion interactions can be included by adding a damped dispersion term as parametrized sum over atom pair C_6 contributions (DFT-D).[10,13,14,16,17] Whether this also works for processes involving bond rearrangements is a

† Hamburg University of Technology.
‡ Humboldt-Universität zu Berlin.
§ University of California, Berkeley.

(1) Yilmaz, B.; Müller, U. *Top. Catal.* **2009**, *52*, 888–895.
(2) Vermeiren, W.; Gilson, J.-P. *Top. Catal.* **2009**, *52*, 1131–1161.
(3) Smit, B.; Maesen, T. L. M. *Chem. Rev.* **2008**, *108*, 4125–4184.
(4) Krishna, R. *J. Phys. Chem. C* **2009**, *113*, 19756–19781.
(5) Wesolowski, T. A.; Parisel, O.; Ellinger, Y.; Weber, J. *J. Phys. Chem. A* **1997**, *101*, 7818–7825.
(6) Zhang, Y.; Pan, W.; Yang, W. *J. Chem. Phys.* **1997**, *107*, 7921–7925.
(7) Gritsenko, O. V.; Ensing, B.; Schipper, P. R. T.; Baerends, E. J. *J. Phys. Chem. A* **2000**, *104*, 8558–8565.
(8) Porezag, D.; Pederson, M. R. *J. Chem. Phys.* **1995**, *102*, 9345–9349.
(9) Tuma, C.; Sauer, J. *Phys. Chem. Chem. Phys.* **2006**, *8*, 3955–3965.
(10) Kerber, T.; Sierka, M.; Sauer, J. *J. Comput. Chem.* **2008**, *29*, 2088–2097.
(11) Zhao, Y.; Truhlar, D. G. *J. Phys. Chem. A* **2005**, *109*, 5656–5667.
(12) Zhao, Y.; Truhlar, D. G. *Acc. Chem. Res.* **2008**, *41*, 157–167.

subject of active research. A further issue with the computational modeling of reactions in zeolites is associated with the description of the long-range crystal potential and steric effects caused by confinement within the pores of these materials. While these effects can be taken into account, in principle, by using large clusters, such calculations often do not converge with increasing cluster size, suggesting that it would be best to use periodic calculations.[9] The method of choice for correctly including both long-range electron correlation as well as the pore topology would be periodic MP2 calculations. However, for periodic systems, MP2 calculations are at present only feasible with small basis sets and for systems containing only a few atoms in the unit cell.[18−20] For accurate calculation of reaction energies and energy barriers in extended systems, hybrid schemes such as the MP2:DFT scheme introduced by Tuma and Sauer[9,21] can be applied. This approach combines MP2 calculations with Gaussian basis sets for the reaction site and plane-wave DFT for the full system under periodic boundary conditions. For a series of cluster models (**C**) a size-dependent "high-level" correction, defined as the difference between MP2 and DFT energies is calculated,

$$\Delta E(\mathbf{C})_{\mathrm{high}} = \Delta E(\mathbf{C})_{\mathrm{MP2}} - \Delta E(\mathbf{C})_{\mathrm{DFT}} \quad (1)$$

and extrapolated to the periodic structure (**S**). This periodic model limit,$\Delta\tilde{E}(\mathbf{S})_{\mathrm{high}}$, is added to the plane-wave DFT energy for the periodic structure, $\Delta E(\mathbf{S})_{\mathrm{DFT}}$, to get an estimate of the MP2 energy for the full periodic system,

$$\Delta\tilde{E}(\mathbf{S})_{\mathrm{MP2}} = \Delta E(\mathbf{S})_{\mathrm{DFT}} + \Delta\tilde{E}(\mathbf{S})_{\mathrm{high}} \quad (2)$$

In eq 2 and throughout this paper we use a tilde to distinguish energies that were obtained through fitting and/or extrapolation from those obtained directly from quantum chemical calculations (MP2, PBE).

This "periodic" MP2 energy, $\Delta\tilde{E}(\mathbf{S})_{\mathrm{MP2}}$, is subsequently corrected for errors due to basis set incompleteness, calculated for cluster models $\mathbf{C}_{\mathrm{CBS}}$, $\Delta E(\mathbf{C}_{\mathrm{CBS}})^{\mathrm{CBS}}_{\mathrm{MP2}}$, as well as for higher -order correlation effects estimated by coupled cluster, CCSD(T), calculations for cluster model $\mathbf{C}_{\mathrm{CC}}$, $\Delta E(\mathbf{C}_{\mathrm{CC}})_{\mathrm{CCSD(T)}}$. The *final estimate* including all of these corrections, $\Delta\tilde{E}(\mathbf{S})_{\mathrm{final\ estimate}}$, is obtained as

$$\Delta\tilde{E}(\mathbf{S})_{\mathrm{final\ estimate}} = \Delta\tilde{E}(\mathbf{S})_{\mathrm{MP2}} + \Delta E(\mathbf{C}_{\mathrm{CBS}})^{\mathrm{CBS}}_{\mathrm{MP2}} + \Delta E(\mathbf{C}_{\mathrm{CC}})_{\mathrm{CCSD(T)}} \quad (3)$$

The hybrid MP2:DFT approach has been applied previously to proton jumps in zeolites,[21] adsorption of isobutene[9] and stability of *tert*-butyl carbenium ion[22] in zeolite H-FER, and methylation of alkenes in H-ZSM-5.[23] In all cases substantial improvement regarding the agreement with experimental data was achieved over pure DFT results.

The hybrid MP2:DFT calculations start with structure optimizations and frequency calculations at the DFT level with periodic boundary conditions. This can be followed by a reoptimization on the hybrid MP2:DFT potential energy surface using the high-level correction for an appropriate cluster size $\mathbf{C}_{\mathrm{OPT}}$ according to

$$\Delta E(\mathbf{S}{:}\mathbf{C})_{\mathrm{MP2:DFT}} = \Delta E(\mathbf{S})_{\mathrm{DFT}} + \Delta E(\mathbf{C}_{\mathrm{OPT}})_{\mathrm{high}} \quad (4)$$

This reoptimization has been carried out in refs 9, 21, 22, but is not done in the present study. Here, we follow ref 23 and evaluate the "periodic" MP2 estimate and the final energy estimate according to eqs 2 and 3 as single-point energies at the DFT optimized structures.

In the present study we employ the MP2:DFT hybrid scheme to revise our previous DFT calculations for the alkylation of benzene with ethene over zeolite H-ZSM-5 which used cluster models of the active site to determine energy barriers and rate coefficients.[24] For the Al12−O20(H)−Si3 site[23,25] (numbering according to ref 26) we considered both a one-step scheme, in which the precursor is represented by coadsorbed ethene and benzene at the acid site and a two-step mechanism in which ethene is first protonated to form an ethoxide species that subsequently reacts with benzene to form the product, ethylbenzene. The rate coefficients for these elementary steps, together with diffusivities obtained from molecular dynamics simulations, were then used in a continuum model of a zeolite crystal to calculate the overall activity as a function of the gas-phase conditions.[27] It turned out, however, that the theoretically determined rate coefficients for the one-step mechanism had to be increased by 2 orders of magnitude to achieve agreement with experimental data, while the rate coefficients for the two-step mechanism had to be lowered by a factor of 4. Moreover, the apparent activation energy determined for the one-step mechanism was too low by 15 kJ/mol, while that for the two-step mechanism was slightly higher than the experimental values. It is therefore reasonable to reconsider the alkylation of benzene using more sophisticated quantum chemical approaches in order to obtain a clearer view of the energetics and kinetics of this reaction.

The present study has two objectives. The first is to use the hybrid MP2:DFT methodology to calculate accurate intrinsic energy barriers for the benzene alkylation with ethene and to derive rate coefficients for all elementary steps which are based on quantum chemical calculations that are converged with respect to both system size and methodology. The second objective is to generate adsorption energies and energy barriers that can be used as benchmarks in the development of computationally less expensive approaches such as hybrid QM: force field methods[25,28,29] or DFT+Dispersion methods.[10,13]

(13) Grimme, S. *J. Comput. Chem.* **2006**, *27*, 1787–1799.
(14) Schwabe, T.; Grimme, S. *Acc. Chem. Res.* **2008**, *41*, 569–579.
(15) Sherrill, C. D.; Takatani, T.; Hohenstein, E. G. *J. Phys. Chem. A* **2009**, *113*, 10146–10159.
(16) Ortmann, F.; Bechstedt, F.; Schmidt, W. G. *Phys. Rev. B* **2006**, *73*, 205101–1/10.
(17) Civalleri, B.; Zicovich-Wilson, C. M.; Valenzano, L.; Ugliengo, P. *Cryst. Eng. Commun.* **2008**, *10*, 405–410.
(18) Maschio, L.; Usvyat, D.; Manby, F. R.; Casassa, S.; Pisani, C.; Schütz, M. *Phys. Rev. B.* **2007**, *76*, 075101–1/9.
(19) Casassa, S.; Halo, M.; Maschio, L.; Roetti, C.; Pisanti, C. *Theor. Chem. Acc.* **2007**, *117*, 781–791.
(20) Pisani, C.; Maschio, L.; Casassa, S.; Halo, M.; Schütz, M.; Usvyat, D. *J. Comput. Chem.* **2008**, *29*, 2113–2124.
(21) Tuma, C.; Sauer, J. *Chem. Phys. Lett.* **2004**, *387*, 388–394.
(22) Tuma, C.; Kerber, T.; Sauer, J. *Angew. Chem., Int. Ed.* **2010**, *49*, 4678–4680.
(23) Svelle, S.; Tuma, C.; Rozanska, X.; Kerber, T.; Sauer, J. *J. Am. Chem. Soc.* **2009**, *131*, 816–825.
(24) Hansen, N.; Brüggemann, T.; Bell, A. T.; Keil, F. J. *J. Phys. Chem. C* **2008**, *112*, 15402–15411.
(25) Clark, L. A.; Sierka, M.; Sauer, J. *J. Am. Chem. Soc.* **2004**, *126*, 936–947.
(26) Olson, D. H.; Koktailo, G. T.; Lawton, S. L.; Meier, W. M. *J. Phys. Chem.* **1981**, *85*, 2238–2243.
(27) Hansen, N.; Krishna, R.; van Baten, J. M.; Bell, A. T.; Keil, F. J. *J. Phys. Chem. C* **2009**, *113*, 235–246.
(28) Clark, L. A.; Sierka, M.; Sauer, J. *J. Am. Chem. Soc.* **2003**, *125*, 2136–2141.

Scheme 1. Elementary Processes Involved in the Alkylation of Benzene with Ethene

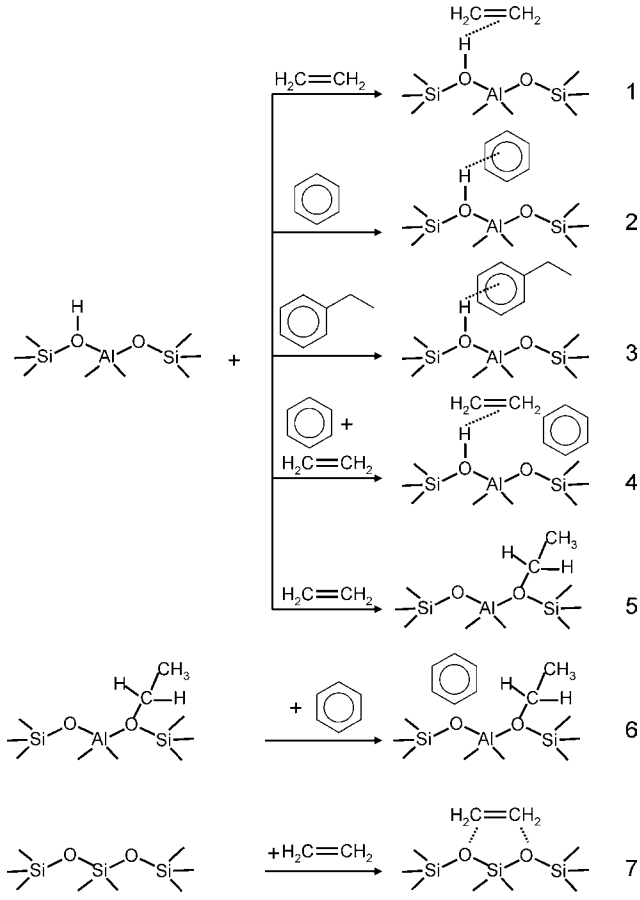

From the different options of the latter,[10] we have selected the pragmatic approach of Grimme, adding a parametrized damped $1/r^6$ term to the DFT energy, because it is easy to implement and easy to evaluate with negligible additional computer time, and a clear protocol is available for parameter generation by DFT.[13]

The elementary processes to which the hybrid MP2:DFT approach was applied are summarized in Scheme 1. Included are physical adsorption of ethene, benzene, and ethylbenzene via π-complex formation with a Brønsted acid site, reactions **1**−**3** in Scheme 1; coadsorption of ethene and benzene on a Brønsted acid site, reaction **4**; reaction of ethene with a Brønsted acid site to form an ethoxide species, reaction **5**; benzene adsorption next to the ethoxide species, reaction **6**; and ethene adsorption in purely siliceous MFI, reaction **7**. Energy barriers and rate coefficients were calculated for the one-step scheme (**1s**) and for both steps of the two-step mechanism (**2s(1)** and **2s(2)**; see ref 24 for details).

2. Computational Details

The *final estimate* adsorption energies and energy barriers were calculated in three steps. First, a structure optimization for the entire H-ZSM-5 unit cell was carried out using DFT with periodic boundary conditions. Note that in contrast to the original approach[9] but following ref 23 hybrid MP2:DFT structure optimization were not performed because of (i) the computational expense of these calculations and (ii) the small effect of high-level structure relaxation effects.[9] Second, single-point MP2 and DFT calculations were conducted on clusters of increasing size cut out from the plane-wave DFT optimized structures to determine the periodic MP2-limit by extrapolation. Third, single-point MP2 calculations with increasing basis set size are performed to determine the complete basis set limit. Additionally, CCSD(T) calculations on small cluster models were carried out, to account for higher-order correlation effects.

2.1. DFT Calculations Applying Periodic Boundary Conditions. DFT calculations applying periodic boundary conditions were performed using the Vienna ab initio simulation program (VASP).[30−33] The gradient-corrected exchange-correlation functional proposed by Perdew, Burke, and Ernzerhof (PBE)[34,35] was employed. Plane-wave calculations were conducted using the projector-augmented wave (PAW) method.[36,37] The plane-wave basis set kinetic energy cutoff was set to 400 eV. Brillouin-zone sampling was restricted to the gamma point. The unit cell parameters α, β, and γ were fixed to 90° in all calculations as no significant deviation from the orthorhombic system is expected.[38−40] To estimate whether the unit cell vector lengths significantly affect adsorption energies and energy barriers, we calculated these properties for some steps using two different sets of cell dimensions. The first set (a = 20.022 Å, b = 19.899 Å, c = 13.383 Å; UC1) comes from crystallographic data,[41] while the second set (a = 20.157 Å, b = 20.033 Å, c = 13.473 Å; UC2) results from optimization of an all-silica unit cell as detailed in ref 23. To create an acidic site, one of the 96 Si atoms in the unit cell was replaced by an Al atom in the T12 site[25] and the resulting negative charge was compensated by a proton bonded to one of the neighboring framework oxygen atoms. Specifically the Al12−O20(H)−Si3 site (numbering according to ref 26) was chosen[23−25] because of its location at the intersection between straight and sinusoidal channels; for details see section S.1 of the Supporting Information.

Minima on the PBE potential energy surface were located using the conjugate gradient algorithm with fully relaxed atomic positions. Convergence was considered to be achieved when forces were below 10^{-4} eV/Å. Energies were converged to 10^{-5} eV in all cases. Transition structures were located by transferring optimized transition structures from our recent cluster study[24] into the periodic environment and reoptimizing them using the improved-dimer method.[42] Transition structures were considered converged when forces on all atoms were smaller than 0.05 eV/Å. Stationary points found were characterized by harmonic frequencies obtained by diagonalization of the full dynamical matrices. The force constants were obtained by numerical differentiation of forces with a step size of 0.02 Å. No scaling factor was applied for the frequencies. DFT energy calculations for gas-phase molecules were carried out using cubic boxes with edge lengths of 25 Å to minimize interactions with the periodic images.[23]

2.2. MP2 and DFT Cluster Calculations. For the evaluation of the high-level correction (eq 1) single-point energy calculations were performed on clusters cut out from the plane-wave DFT-

(29) De Moor, B. A.; Reyniers, M.-F.; Sierka, M.; Sauer, J.; Marin, G. B. *J. Phys. Chem. C* **2008**, *112*, 11796–11812.
(30) Kresse, G.; Hafner, J. *Phys. Rev. B* **1993**, *48*, 13115–13126.
(31) Kresse, G.; Hafner, J. *Phys. Rev. B* **1994**, *49*, 14251–14296.
(32) Kresse, G.; Furthmüller, J. *J. Comput. Mater. Sci.* **1996**, *6*, 15–50.
(33) Kresse, G.; Furthmüller, J. *Phys. Rev. B* **1996**, *54*, 11169–11186.
(34) Perdew, J. P.; Burke, K.; Ernzerhof, M. *Phys. Rev. Lett.* **1996**, *77*, 3865–3868.
(35) Perdew, J. P.; Burke, K.; Ernzerhof, M. *Phys. Rev. Lett.* **1997**, *78*, 1396.
(36) Blöchl, P. E. *Phys. Rev. B* **1994**, *50*, 17953–17979.
(37) Kresse, G.; Joubert, D. *Phys. Rev. B* **1999**, *59*, 1758–1775.
(38) Hay, D. G.; Jaeger, H.; West, G. W. *J. Phys. Chem.* **1985**, *89*, 1070–1072.
(39) van Koningsveld, H.; Jansen, J. C.; van Bekkum, H. *Zeolites* **1987**, *7*, 564–568.
(40) van Koningsveld, H. *Acta Crystallogr.* **1990**, *B46*, 731–735.
(41) van Koningsveld, H. *Acta Crystallogr.* **1987**, *B43*, 127–132.
(42) Heyden, A.; Bell, A. T.; Keil, F. J. *J. Chem. Phys.* **2005**, *123*, 224101–1/14.

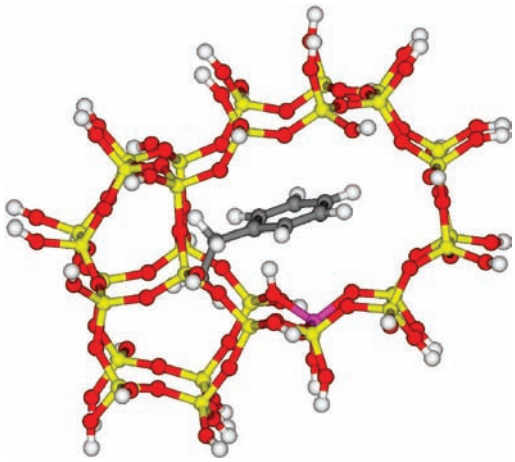

Figure 1. The largest system calculated with MP2/TZVP(P) in the present work is the 30T cluster with the overall composition $C_8H_{53}O_{81}Si_{29}Al$ (here: adsorbed ethylbenzene, viewed along the straight channel). Color codes: oxygen (red), silicon (yellow), aluminum (pink), hydrogen (white), carbon (gray).

optimized periodic structures. A series of 16 cluster models of increasing size was constructed for all stationary points with the largest cluster containing 30 T-atoms. The cluster models were saturated with hydrogen atoms such that the terminating groups were SiO-H (r(O−H) = 0.967 Å) or AlO-H (r(O−H) = 0.963 Å).[43] Figure 1 shows adsorbed ethylbenzene as an example for the largest system considered.

For each cluster model and gas phase molecule, MP2 energies were computed with the TURBOMOLE program package[44−46] using basis sets of triple-ζ quality.[47] For carbon atoms and those oxygen atoms which connect two T-atoms (T−O−T) the TZVPP basis set was chosen while for all other atoms the TZVP basis set was used. Following Tuma and Sauer[9] we denote this combination as TZVP(P) in the remainder of this paper. Electrons in molecular orbitals corresponding to C 1s, O 1s, Al 1s, and Si 1s atomic orbitals were excluded from the MP2 correlation scheme.

DFT energies for each cluster model and gas-phase molecule were computed within the RI approximation[48−50] using the PBE functional[34,35] and a basis set of quadruple-ζ quality (def2-QZVP).[51] Energies were not corrected for BSSE which is expected to be negligible for this basis set. The employment of Gaussian type orbitals (GTO) as basis sets for this part of the hybrid method differs from previous studies where the PBE energies for all cluster models have been obtained with the same plane-wave methodology as was used for the periodic structure.[9,23] Comparison of adsorption energies for ethene adsorption on the acid site for several cluster models showed energy differences below 0.5 kJ/mol between both approaches.

The differences between MP2 and PBE adsorption energies converge monotonically with the cluster size $\mathbf{C}_n$ (see below) and can be extrapolated to the periodic limit using the following analytical expression:[9]

$$E^{\mathrm{fit}}_{\mathrm{HL\text{-}corr}}(n) = E_{\mathrm{disp}}(n) + E_{\mathrm{add}} \tag{5}$$

It consists of an additive constant, E_{add}, which accounts for all effects contributing to MP2-PBE adsorption energy differences that do not strongly depend on the cluster size, for example the self-interaction correction (SIC) error, and a term

$$E_{\mathrm{disp}}(n) = -s_6 \sum_{i}^{N_{n-1}} \sum_{j=i+1}^{N_n} \frac{\sqrt{C_6^i \cdot C_6^j}}{R_{ij}^6} f_{\mathrm{d}}(R_{ij}) \tag{6}$$

which has the analytical form of a sum over damped atomic C_6 dispersion contributions for all atom pairs i and j at distance R_{ij}. N_n denotes the number of atoms in cluster $\mathbf{C}_n$. For the damping function $f_d(R_{ij})$ we use the functional form and the parameter values proposed by Grimme.[13] The global scaling parameter, s_6, depends on the particular exchange-correlation functional. For the PBE functional its value is 0.75.[13] The five atomic C_6 coefficients, C_6^i, and the additional constant, E_{add}, are fitted for each reaction individually by minimizing

$$\Delta(\{C_6^i\}, E_{\mathrm{add}}) = \sum_{n=1}^{n_{\max}} \left[(\Delta E(n)_{\mathrm{MP2}} - \Delta E(n)_{\mathrm{PBE}}) - E^{\mathrm{fit}}_{\mathrm{HL\text{-}corr}}(n) \right]^2 \tag{7}$$

using a series of $n_{\max}$ cluster models $\mathbf{C}_n$ of increasing size. The parameters obtained are given in Table S.6 of the Supporting Information. Using the fitted C_6 parameters,$E_{\mathrm{disp}}(\mathbf{S})$is obtained by applying eq 6 to the periodic structure by means of lattice sums.[10] The high-level correction for the periodic system **S**,

$$\Delta\tilde{E}(\mathbf{S})_{\mathrm{high}} = \Delta\tilde{E}(\mathbf{S})_{\mathrm{MP2}} - \Delta E(\mathbf{S})_{\mathrm{PBE}} \approx E_{\mathrm{disp}}(\mathbf{S}) + E_{\mathrm{add}} \tag{8}$$

has then to be added to the periodic DFT result, $\Delta E(\mathbf{S})_{\mathrm{PBE}}$, to get estimates for the full "periodic" MP2 adsorption energies, $\Delta\tilde{E}(\mathbf{S})_{\mathrm{MP2}}$that has been introduced in eq 2.

The same procedure is applied to the apparent energy barriers which also show a monotonic decay. They are fitted according to eq 7 and extrapolated to the periodic limit. The fit parameters obtained are given in Table S.7 of the Supporting Information. In contrast, the high-level corrections for the intrinsic barriers have been obtained as difference of the high-level corrections of the apparent barriers and the respective adsorbate complexes. As shown in section S.7 of the Supporting Information, the differences between MP2 and PBE results for the intrinsic energy barriers depend only weakly on the cluster size and do not show a monotonic decay with increasing cluster size which makes fitting and direct extrapolation less reliable.

2.3. Complete Basis Set Extrapolation. The incompleteness of Gaussian basis sets introduces an error in the MP2 calculations that can be accounted for approximately by extrapolation to the complete basis set (CBS) limit. BSSE-corrected[52] RI-MP2 single-point energies obtained using Dunning's correlation consistent polarized valence triple-ζ and quadruple-ζ basis sets cc-pVXZ (X = 3 and 4)[53,54] were used for this purpose. Extrapolation to the CBS limit assumes an exponential behavior of the Hartree−Fock energy and an X^{-3} behavior of the correlation energy as a function of the basis set cardinal number X (=3,4), see section S.2 of the Supporting Information for more details.

The CBS limit correction,$\Delta E(\mathbf{C}_{\mathrm{CBS}})^{\mathrm{CBS}}_{\mathrm{MP2}}$,

(43) Sierka, M.; Sauer, J. *Faraday Discuss.* **1997**, *106*, 41–62.
(44) Ahlrichs, R.; Bär, M.; Häser, M.; Horn, H.; Kölmel, C. *Chem. Phys. Lett.* **1989**, *162*, 165–169.
(45) Hättig, C. *J. Chem. Phys.* **2003**, *118*, 7751–7761.
(46) Hättig, C.; Hellweg, A.; Köhn, A. *Phys. Chem. Chem. Phys.* **2006**, *8*, 1159–1169.
(47) Schäfer, A.; Huber, C.; Ahlrichs, R. *J. Chem. Phys.* **1994**, *100*, 5829–5835.
(48) Eichkorn, K.; Treutler, O.; Öhm, H.; Häser, M.; Ahlrichs, R. *Chem. Phys. Lett.* **1995**, *240*, 283–290.
(49) Eichkorn, K.; Treutler, O.; Öhm, H.; Häser, M.; Ahlrichs, R. *Chem. Phys. Lett.* **1995**, *242*, 652–660.
(50) Eichkorn, K.; Weigend, F.; Treutler, O.; Ahlrichs, R. *Theor. Chem. Acc.* **1997**, *97*, 119–124.
(51) Weigend, F.; Furche, F.; Ahlrichs, R. *J. Chem. Phys.* **2003**, *119*, 12753–12762.
(52) Boys, S. F.; Bernardi, F. *Mol. Phys.* **1970**, *19*, 553–566.
(53) Dunning, T. H. *J. Chem. Phys.* **1989**, *90*, 1007–1023.
(54) Woon, D. E.; Dunning, T. H. *J. Chem. Phys.* **1993**, *98*, 1358–1371.

$$\Delta E(\mathbf{C}_{\mathrm{CBS}})_{\mathrm{MP2}}^{\mathrm{CBS}} = \left(\Delta E(\mathbf{C}_{\mathrm{CBS}})_{\mathrm{HF}}^{\mathrm{CBS}} + \Delta E(\mathbf{C}_{\mathrm{CBS}})_{\mathrm{corr}}^{\mathrm{CBS}}\right) - \left(\Delta E(\mathbf{C}_{\mathrm{CBS}})_{\mathrm{HF}}^{\mathrm{TZVP(P)}} + \Delta E(\mathbf{C}_{\mathrm{CBS}})_{\mathrm{corr}}^{\mathrm{TZVP(P)}}\right) \quad (9)$$

is the difference between BSSE-corrected adsorption energies extrapolated to the complete basis set limit and BSSE-uncorrected adsorption energies obtained with the TZVP(P) basis set calculated for cluster model $\mathbf{C}_{\mathrm{CBS}}$. $\Delta E(\mathbf{C}_{\mathrm{CBS}})_{\mathrm{MP2}}^{\mathrm{CBS}}$ is added to $\Delta \tilde{E}(\mathbf{S})_{\mathrm{MP2}}$ obtained from eq 8 to get a BSSE-free MP2 adsorption energy for the periodic structure. For $\mathbf{C}_{\mathrm{CBS}}$ we adopt the T18 cluster model, except for the coadsorption of ethene and benzene for which the T16 cluster is adopted because of the high computational costs associated with a 3-body counter-poise correction. In section S.2 of the Supporting Information we show that from the 16T−18T size region on, the CBS limit correction can be assumed constant.

The CBS limit corrections for intrinsic energy barriers were obtained indirectly from the CBS limit corrections of the apparent energy barriers and those of the associated adsorbate complex.

2.4. CCSD(T) Calculations. The reliability of MP2 to predict adsorption energies and energy barriers for the alkylation was assessed by performing single-point CCSD(T) calculations for all stationary points on a modified 3T cluster model. This modified model was obtained from the 3T model used in the cluster series calculations by replacement of SiO−H by Si−H terminations with a Si−H bond length of 1.455 Å[23] (see Figure 2) to reduce the computational expenses. In section S.4 of the Supporting Information we show, by evaluating MP2/CBS-PBE+D energies as function of the cluster size, that higher-order correlation effects depend only weakly on the cluster size, leading us to conclude that a relatively small cluster model is sufficient. The CCSD(T) calculations were carried out with the MOLPRO code[55] employing Ahlrich's improved triple-ζ valence basis set (def2-TZVP)[56] for all atoms. For our *final estimates* of adsorption energies and energy barriers we add the difference between CCSD(T) and RI-MP2 adsorption energies and energy barriers calculated on the same 3T cluster, $\Delta E(\mathbf{C}_3)_{\mathrm{CCSD(T)}}$, to the "periodic" MP2 adsorption energies and energy barriers.

2.5. PBE+D//PBE Calculations. With PBE+D//PBE we denote the evaluation of the energy of plane-wave DFT-optimized structures according to

$$E(\mathbf{S})_{\mathrm{PBE+D//PBE}} = E(\mathbf{S})_{\mathrm{PBE}} + E_{\mathrm{disp}}(\mathbf{S}) \quad (10)$$

with the dispersion term given in eq 6 using the *transferable* C_6-coefficients of Grimme.[13] Adsorption energies calculated in this way still contain the self-interaction error but are significantly less expensive to obtain than those determined from the full MP2:DFT calculation because eq 6 can be applied directly to the periodic unit cell optimized by plane-wave DFT. By doing so the computationally expensive determination of MP2 and DFT adsorption energies for a series of clusters as well as the basis set limit extrapolation procedure are avoided. It is therefore of great interest to evaluate further the transferability of the C_6-coefficients published by Grimme[13] to solid state and surface problems.[10]

2.6. Calculation of Intrinsic Rate Coefficients. Intrinsic rate coefficients are calculated from conventional transition state theory,[57,58]

$$k(T) = \sigma \frac{k_{\mathrm{B}}T}{h}\frac{Q_{\mathrm{TS}}(T)}{Q_{\mathrm{R}}(T)}\exp[-E^{\ddagger}/RT] \quad (11)$$

where k_{B} is Boltzmann's constant, h is Planck's constant, T is the absolute temperature, and $E^{\ddagger}$is the difference in electronic energies between the transition state and the reactant state. With σ we denote a reaction path symmetry number,[59] while Q_{TS} and Q_{R} are the partition functions of the transition state and the reactant state, respectively. The most straightforward method to calculate the partition functions is to assume immobile adsorption, that is, a complete conversion of frustrated rotational and translational degrees of freedom into vibrations. However, contributions from low vibrational modes corresponding to rotational and translational movements of adsorbate molecules are often not adequately taken into account by this treatment[60] and may lead to an underestimation of the partition function. As is shown in section S.5 of the Supporting Information, the assumption of immobile adsorption is a reasonable approximation for both the one-step mechanism and the elementary steps of the two-step mechanism.

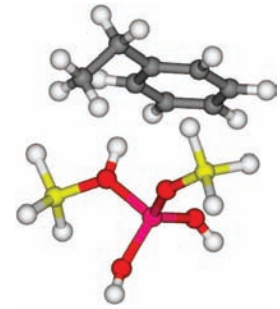

Figure 2. The largest system calculated with CCSD(T)/def2-TZVP in the present work is the 3T cluster with the overall composition $C_8H_{19}O_4Si_2Al$ (here: adsorbed ethylbenzene). Color codes: oxygen (red), silicon (yellow), aluminum (pink), hydrogen (white), carbon (gray).

3. Results and Discussion

3.1. Adsorption of Reactants and Products. 3.1.1. Periodic DFT Structure Optimization. The first row of Table 1 shows the PBE interaction energies for all adsorbate molecules obtained with the UC1 set of cell parameters. The size of the unit cell affects the physisorption energies by up to 5 kJ/mol (see section S.6.1 of the Supporting Information for a detailed discussion). The orientation of all adsorbates within the unit cell is shown in Figure 3. The absence of imaginary frequencies confirmed that all stationary points were true minima. The zero-point vibrational energies calculated from these PBE frequencies are also shown in Table 1 (seventh row). The calculated wavenumber for the O−H stretching mode is 3705 cm^{-1} (H on O20) in good agreement with other theoretical studies on H-FER (3680 cm^{-1})[61] and H-MOR (3709 cm^{-1})[62] employing similar plane wave calculations. A change in the unit cell parameters affects the O−H stretching mode by just 4 cm^{-1}. The calculated frequencies are larger than the experimental wave numbers of 3623 cm^{-1} (at 170 K)[63] and 3612 cm^{-1} (at 300 K),[63,64] as expected, due to the limited accuracy of harmonic DFT force constants and neglect of anharmonicities. The calculated red-shifts of the O−H stretching modes induced by adsorption of ethene and benzene, −535 cm^{-1} and −498 cm^{-1}, respectively,

(55) Werner, H.-J.; et al. *MOLPRO: A package of ab initio programs*, version 2006.1; Cardiff: UK, 2006.
(56) Weigend, F.; Ahlrichs, R. *Phys. Chem. Chem. Phys.* **2005**, *7*, 3297–3305.
(57) Eyring, H. *J. Chem. Phys.* **1935**, *3*, 107–115.
(58) Evans, M. G.; Polanyi, M. *Trans. Faraday Soc.* **1935**, *31*, 875–894.
(59) Fernándes-Ramos, A.; Ellington, B. A.; Meana-Pañeda, R.; Marques, J. M. C.; Truhlar, D. G. *Theor. Chem. Acc.* **2007**, *118*, 813–826.
(60) De Moor, B. A.; Reyniers, M.-F.; Marin, G. B. *Phys. Chem. Chem. Phys.* **2009**, *11*, 2939–2958.
(61) Tuma, C. A QM/QM hybrid method for MP2/plane-wave-DFT studies of extended systems. Ph.D. Thesis Humboldt-Universität Berlin, 2006.
(62) Bučko, T.; Benco, L.; Demuth, T.; Hafner, J. *J. Chem. Phys.* **2002**, *117*, 7295–7305.
(63) Trombetta, M.; Armaroli, T.; Gutierrez Alejandre, A.; Ramirez Solis, J.; Busca, G. *Appl. Catal., A* **2000**, *192*, 125–136.
(64) Zecchina, A.; Spoto, G.; Bordiga, S. *Phys. Chem. Chem. Phys.* **2005**, *7*, 1627–1642.

Table 1. Adsorption Energies Obtained Using the Hybrid MP2:DFT Scheme and PBE+D Adsorption Energies at the PBE Optimized Structures As Predicted by the Parameters of Grimme[13a]

	1	2	3	4	5	6	7[b]
$\Delta E(\mathbf{S})_{\mathrm{PBE}}$	−31.5	−24.0	−16.6	−40.7	−53.5	−2.0	−4.2
$\Delta\tilde{E}(\mathbf{S})_{\mathrm{high}}$	−26.7[c]	−76.2[d]	−118.3	−122.6	−27.5	−95.8	−20.5
$\Delta E(\mathbf{C}_{18})_{\mathrm{MP2}}^{\mathrm{CBS}}$	5.8	14.2	13.8	14.8[e]	12.9	11.7	7.7
$\Delta E(\mathbf{C}_3)_{\mathrm{CCSD(T)}}$[f]	4.1	5.5	6.1	7.5	6.9	3.9	0.5
$\Delta\tilde{E}(\mathbf{S})_{\mathrm{final\ estimate}}$	−48.3	−80.5	−115.1	−141.0	−61.3	−82.2	−16.5
difference to PBE	−16.8	−56.5	−98.5	−100.3	−7.7	−80.2	−12.3
$\Delta E(\mathbf{S})_{\mathrm{ZPV}}$	1.4	−0.2	2.8	6.4	10.5	4.1	−1.9
$\Delta H(\mathbf{S})_{298} - \Delta E_0(\mathbf{S})_{\mathrm{PBE}}$[g]	1.1	2.6	2.3	3.9	−2.6	3.0	4.7
$\Delta H(\mathbf{S})_{653} - \Delta E_0(\mathbf{S})_{\mathrm{PBE}}$[h]	6.5	8.5	7.2	14.2	0.3	8.5	11.6
$\Delta E(\mathbf{S})_{\mathrm{D//PBE}}$	−29.2	−63.0[I]	−100.8	−97.7	−33.7	−73.6	−18.8
$\Delta E(\mathbf{S})_{\mathrm{PBE+D//PBE}}$	−60.6	−86.9	−117.4	−138.3	−87.3	−75.6	−23.0
$\Delta E(\mathbf{C}_{18})_{\mathrm{high}}^{\mathrm{DFT+D}}$	1.2	−11.4	−12.1	−10.9[e]	3.2	−11.7	−2.7
$\Delta E(\mathbf{S})_{\mathrm{final\ estimate}}^{\mathrm{DFT+D}}$	−49.5	−78.7	−109.6	−126.9	−64.3	−71.7	−17.5

[a] Zero-point vibrational energies and thermal contributions to adsorption enthalpies are also included. Energies are reported in kJ/mol. [b] Adsorption in channel intersection. [c] This values remains the same for Al−O−Si(OH)$_3$ instead of Al−O−H termination. [d] −76.5 kJ/mol for the second set of unit cell parameters. [e] For 16T cluster. [f] Difference between CCSD(T) and RI-MP2 adsorption energies on a 3T cluster. [g] Contribution to enthalpy at 298 K ($\Delta E_0(\mathbf{S})_{\mathrm{PBE}}$ is the ZPVE corrected adsorption energy). [h] Contribution to enthalpy at 653 K ($\Delta E_0(\mathbf{S})_{\mathrm{PBE}}$ is the ZPVE corrected adsorption energy). [I] −60.9 kJ/mol for the second set of unit cell parameters.

are larger than the experimental values of −398 cm^{-1} (ref 65) and −360 cm^{-1} (ref 66), which is also a known characteristic of gradient corrected functionals in general and PBE in particular.[67] However, the difference of −38 cm^{-1} between the experimentally observed red-shifts for ethene and benzene adsorption is predicted well by the calculated value (−38 cm^{-1}) leading us to conclude that the calculated adsorption complexes are reasonable representations of the precursors at the acid site.

3.1.2. Cluster Model Convergence. Figure 4 shows the results of the single-point MP2 and PBE cluster calculations. The adsorption energies do not show a systematic behavior as a function of the cluster size. Up to a certain cluster size the adsorption energies become more negative and then less negative. Neither the size of the cluster at which the energies have their lowest value nor the magnitude by which the energies increase again seems to be predictable. If, however, the high-level correction is plotted, that is, the difference between MP2 and PBE adsorption energies, $\Delta E(\mathbf{C})_{\mathrm{MP2}} - \Delta E(\mathbf{C})_{\mathrm{PBE}}$, decreasing curves are obtained that converge asymptotically (see Figures 5 and 6). With the exceptions of ethene physisorption and chemisorption (ethoxide formation), the decay is monotonic. These adsorption energy differences are used for fitting the analytical expression given in eq 6. The high-level corrections $\Delta\tilde{E}(\mathbf{S})_{\mathrm{high}}$ are summarized in row 2 of Table 1. Additional calculations addressing the influence of the cluster termination and the size of the unit cell from which the clusters were cut out, revealed that the high-level corrections are insensitive toward these issues (see section S.7 of the Supporting Information for a detailed discussion).

3.1.3. Extrapolation to the Complete Basis Set Limit. The CBS-limit corrections evaluated according to eq 9 for 18T cluster models (16T in case of ethene-benzene coadsorption) are listed in the third row of Table 1.

3.1.4. CCSD(T) Corrections. The CCSD(T) corrections are listed in the fourth row of Table 1. Compared to the previous application of the hybrid scheme to the protonation of isobutene in zeolite ferrierite,[9] the CCSD(T) corrections computed in the present work are always positive. It should be noted that the CCSD(T) correction as defined above contains two contributions, the difference between CCSD(T) and canonical MP2 adsorption energies which are obtained along the CCSD(T) calculations and the difference between canonical MP2 results and the RI-MP2 results. The latter difference is less or equal to 2 kJ/mol. Consequently, the "real" CCSD(T) corrections to the MP2:DFT adsorption energies are less than 8%. This is somewhat larger than in former applications of the hybrid scheme[9,23] and might be attributed to the known tendency of MP2 to overrate electron correlation effects in unsaturated systems and complexes.[68] Therefore, the calculation of CCSD(T) corrections is an essential part of the hybrid approach in the present case.

3.1.5. Final Estimates of Adsorption Energies and Comparison with Experimental Data. The final estimates of the hybrid MP2:DFT adsorption energies are obtained from the sum of the PBE energy, the high-level correction extrapolated to the periodic limit, the complete basis set limit (CBS) correction, and the CCSD(T) corrections, eq 3. Table 1 summarizes all of these contributions. The differences between the final estimates and the PBE results are substantial. For the physisorption structures **1**−**4** and **6**−**7** they are between 6.2 and 13.4 kJ/mol per CH_n unit. For ethylbenzene (**3**) and the coadsorption of ethene and benzene (**4**) the total difference is as large as 100 kJ/mol. There are not only substantial quantitative changes, but also qualitative ones. PBE predicts the counterintuitive sequence ethene > benzene > ethylbenzene for the adsorption strength, whereas our final estimates reverse this sequence.

Before we compare with experiment, we will make an attempt to determine the uncertainty of our *final estimates*. Different choices of the unit cell size in the DFT/plane-wave structure optimization lead to differences of up to around 5 kJ/mol in the adsorption energy. The use of DFT/plane-wave structures instead of reoptimizing the structures at the hybrid MP2:DFT level may lead to changes of up to 10 kJ/mol, as we learn from comparing DFT and DFT+D optimization results.[10] Additional

(65) Spoto, G.; Bordiga, S.; Ricciardi, G.; Scarano, D.; Zecchina, A.; Borello, E. *J. Chem. Soc. Faraday Trans.* **1994**, *90*, 2827–2835.
(66) Mukti, R. R.; Jentys, A.; Lercher, J. A. *J. Phys. Chem. C* **2007**, *111*, 3973–3980.
(67) Tuma, C.; Boese, A. D.; Handy, N. C. *Phys. Chem. Chem. Phys.* **1999**, *1*, 3939–3947.
(68) Schwabe, T.; Grimme, S. *J. Phys. Chem A* **2009**, *113*, 3005–3008.

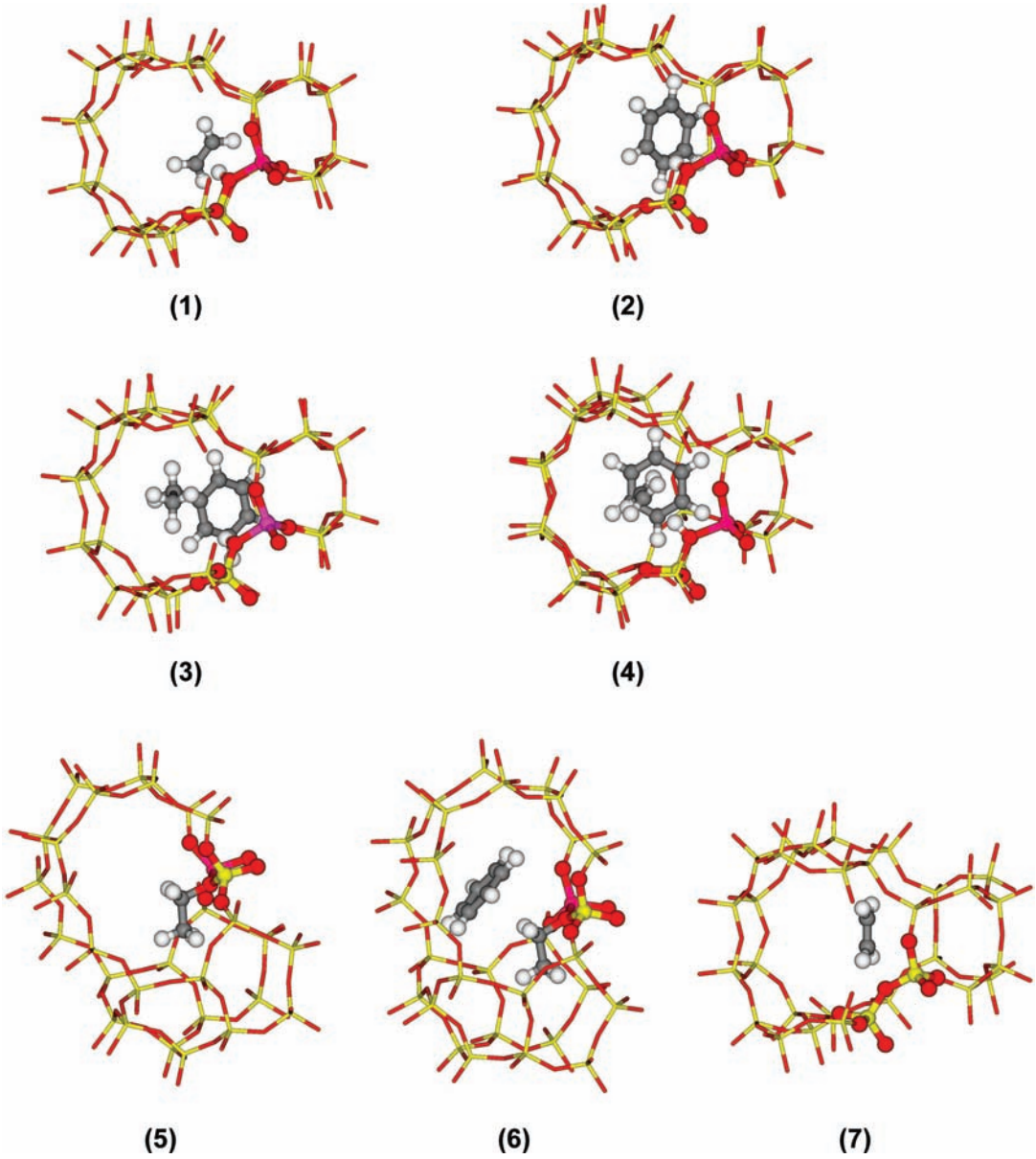

Figure 3. Adsorbed ethene, benzene, and ethylbenzene (1−3), coadsorbed ethene and benzene (4), ethoxide (5), benzene adsorbed next to ethoxide (6), and ethene adsorbed in the channel intersection of all-silica MFI (7).

uncertainties are introduced by the fitting procedure and the extrapolation to the CBS limit. The maximum deviation between the reference data points and the fitted values are 3.7 kJ/mol (see Table S.6 of the Supporting Information). Following ref 23 we estimate the uncertainty in the CBS limit to ±2.5 kJ/mol. As a conservative assumption, a range of ±10 kJ/mol accounts for all uncertainties of our methodology, in agreement with previous applications of the hybrid MP2:DFT approach.[9,23]

Table 2 compares adsorption enthalpies calculated from our *final estimates* by adding the zero-point vibrational energies and thermal corrections evaluated from PBE frequencies with available experimental data. Experimental heats of adsorption for ethene in acidic H-ZSM-5 are not available directly. The calculated enthalpy of adsorption at the acid site, −45.8 kJ/mol, is compared with the experimental value for an H,Na-Y zeolite.[69] Adsorption enthalpies in the aluminum-free analogue, silicalite-1, are ranging from −24 to −31 kJ/mol (see ref 70 and references therein). For ethene, adsorption in the channel intersections is not most favorable. Additional PBE+D//PBE calculations for two representative adsorption sites in the sinusoidal and straight channel yield −32.9 and −30.0 kJ/mol, respectively. If the difference of 9.9 kJ/mol between the sinusoidal channel and the intersection is added to the *final estimate* for the channel intersection, an ΔH value of −23.6 kJ/mol is obtained.

For benzene adsorption in H-ZSM-5, the most reliable experimental result (calorimetry, ref 71) is −63.6 kJ/mol. Other results are ranging from −59.0 to −69.0 kJ/mol (see ref 24 and references therein) indicating an uncertainty range of ±5

(69) Cant, N. W.; Hall, W. K. *J. Catal.* **1972**, *25*, 161–172.
(70) Jakobtorweihen, S.; Hansen, N.; Keil, F. J. *Mol. Phys.* **2005**, *103*, 471–489.
(71) Thamm, H.; Jerschkewitz, H.-G.; Stach, H. *Zeolites* **1988**, *8*, 151–153.
(72) Niessen, W.; Karge, H. G.; Jozefowicz, L. *Stud. Surf. Sci. Catal.* **1993**, *80*, 475–481.
(73) Thamm, H.; Stach, H.; Fiebig, W. *Zeolites* **1983**, *3*, 95–97.

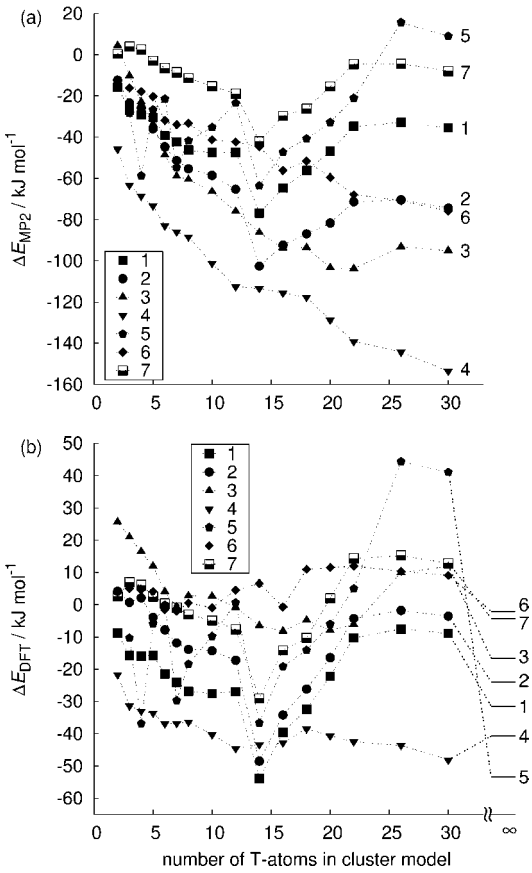

Figure 4. Adsorption energies obtained from single-point energy calculations on cluster models of increasing size. (a) MP2/TZVP(P) results. (b) DFT (PBE/QZVP) results. The periodic model limit is included for comparison.

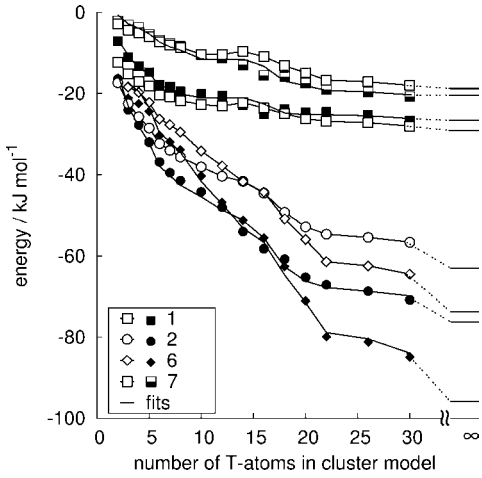

Figure 5. Differences in adsorption energies between MP2 and PBE (filled and partly filled symbols) and dispersion contributions to the adsorption energies as predicted by the parameter set published by Grimme[13] (open symbols). Extrapolations to the full periodic limit are also included.

kJ/mol. The experimental enthalpy of adsorption for ethylbenzene, (−87 kJ/mol, ref 72), is 23 kJ/mol more negative than that for benzene.

The calculated adsorption enthalpies for ethene, isobutene (refs 9, 22), benzene and ethylbenzene are more negative by 8, 10−14, 14, and 23 kJ/mol, respectively, than the experimental values. This small (2−4 kJ/mol per CH_n unit) and systematic overestimation of the strength of the binding to the Brønsted

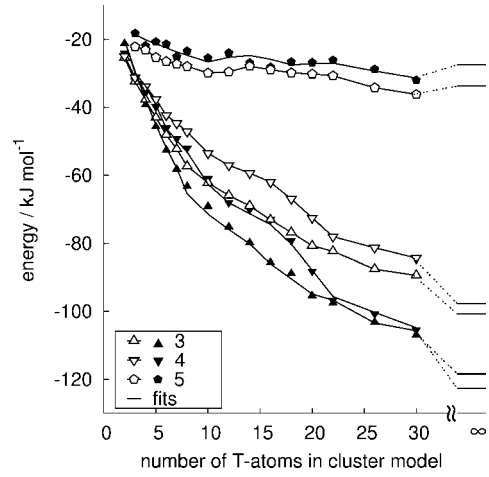

Figure 6. Differences in adsorption energies between MP2 and PBE (filled symbols) and dispersion contributions to the adsorption energies as predicted by the parameter set published by Grimme[13] (open symbols). Extrapolations to the full periodic limit are also included.

acid site we ascribe to remaining uncertainties in our methodology. Moreover, our calculated values refer to one particular site chosen such that the adsorbate can maximize its interaction with the acid site on the zeolite surface (channel intersection), whereas the experimental sample contains a distribution of sites over different crystallographic positions, and these sites are not ordered into unit cells. Compared to previous B3LYP T33 cluster results for ethene, benzene, and ethylbenzene,[24] which were respectively 3, 24, and 48 kJ/mol too small (in absolute terms) our *final estimate* adsorption enthalpies are substantially improved.

3.2. Reaction Steps. 3.2.1. Periodic DFT Structure Optimization. The first row of Table 3 shows the PBE energy barriers for all forward and reverse reactions obtained with the UC1 set of cell parameters. The energy barriers for the reverse reactions '1s, rev' and '2s(2), rev' were calculated with respect to structure 3 shown in Figure 3. The energy barrier for the reverse reaction '2s(1), rev' was calculated with respect to structure 5 shown in Figure 3. The size of the unit cell only affects the second barrier of the two-step scheme by 6.1 kJ/mol. The influence of the unit cell size on ZPVE and thermal contributions is below 2 kJ/mol (see section S.6.2 of the Supporting Information for a detailed discussion). The frequency analysis revealed the presence of exactly one imaginary frequency for all transition structures, which are illustrated in Figure 7.

3.2.2. Cluster Model Convergence. Figure 8 shows the cluster size dependence of the apparent energy barriers, $E^{\ddagger}_{app}$(**C**), for forward and reverse reaction steps obtained from single-point MP2 and PBE cluster calculations. Note that for the first step of the two-step mechanism an apparent energy barrier for the reverse reaction is not required because the intrinsic barrier is calculated from the apparent energy barrier of the forward reaction and the reaction energy for ethoxide formation from the unloaded zeolite cluster and ethene in the gas phase. For the second step of the two-step mechanism we calculated the apparent energy barrier of the forward reaction with respect to the unloaded zeolite cluster and ethene and benzene in the gas phase and not with respect to ethoxide and benzene in the gas phase because a better fit of the MP2-PBE difference was achieved for the former choice. In contrast to the adsorption energies, the apparent energy barriers decrease uniformly with increasing cluster size. However, even for the largest cluster

Table 2. Comparison of Calculated Adsorption Energies and Enthalpies with Experiments (in kJ/mol)

		PBE+D	final estimate		
		$-\Delta E$	$-\Delta E$	$-\Delta H$	obsd
ethene	MFI, sinusoidal channel	32.9		(23.6)[g]	24−31[a]
	MFI, intersection	23.0	16.5	13.7	
	H-MFI, Al12−O20(H)−Si3	60.6	48.3	45.8	38[b]
benzene	H-MFI, Al12−O20(H)−Si3	86.9	80.5	78.1	63.6[c] 64 ± 5[d]
ethylbenzene	H-MFI, Al12−O20(H)−Si3	117.4	115.1	110.0	87 ± 5[d]
isobutene	FER	65.7[i]		(48.1)[h]	49[e]
isobutene	H-FER	90.5[k]	77.2[k]	72.9[k]	59−63[f]

[a] See ref 70 for original references. [b] H,Na-Y zeolite, ref 69. [c] Calorimetry, 1 molecule/unit cell, Si/Al = 86, ref 71. [d] 2 molec/uc, Si/Al = 34, but large amounts of extraframework Al, ref 72. [e] But-1-ene in MFI (silicalite-1), ref 73. [f] Estimated, see ref 9. [g] Estimated from PBE+D difference to intersection and the *final estimate* for the latter. [h] Estimated from PBE+D difference to H-FER and the *final estimate* for the latter. [i] Reference 10. [k] References 9, 22.

Table 3. Intrinsic Energy Barriers Obtained Using the Hybrid MP2:DFT Scheme and PBE+D Intrinsic Energy Barriers at the PBE Optimized Structures As Predicted by the Parameters of Grimme[13a]

	1s	1s, rev	2s(1)	2s(1), rev	2s(2)	2s(2), rev
$E^{\ddagger}(\mathbf{S})_{\mathrm{PBE}}$	84.3	173.1	91.6	113.7	95.9	169.9
$\Delta\tilde{E}^{\ddagger}(\mathbf{S})_{\mathrm{high}}$	43.9	58.1	39.3	40.2	7.4	21.1
$\Delta E^{\ddagger}(\mathbf{C}_{16})^{\mathrm{CBS}}_{\mathrm{MP2}}$	1.0	2.5	0.6[c]	−6.5[c]	0.2	10.4
$\Delta E^{\ddagger}(\mathbf{C}_3)_{\mathrm{CCSD(T)}}$[b]	0.5	−12.8	−1.9	−4.7	−1.0	−11.0
$\tilde{E}^{\ddagger}(\mathbf{S})_{\mathrm{final\ estimate}}$	129.7	220.9	129.7	142.7	102.5	190.3
difference to PBE	45.4	47.8	38.1	29.0	6.6	20.4
$\Delta E^{\ddagger}(\mathbf{S})_{\mathrm{ZPV}}$	−4.8	−14.7	−2.4	−11.4	−5.0	−6.7
$H^{\ddagger}(\mathbf{S})_{653} - E_0^{\ddagger}(\mathbf{S})_{\mathrm{PBE}}$[d]	−7.7	−0.4	−8.6	−2.5	−3.8	−1.9
$\Delta E^{\ddagger}(\mathbf{S})_{\mathrm{D//PBE}}$	−14.4	2.1	−7.5	−3.0	−22.7	−15.9
$E^{\ddagger}(\mathbf{S})_{\mathrm{PBE+D//PBE}}$	69.9	175.3	84.1	110.7	73.2	154.0
$\Delta E^{\ddagger}(\mathbf{C}_{16})^{\mathrm{DFT+D}}_{\mathrm{high}}$	56.0	62.7	53.9	51.6	35.1	42.2
$E^{\ddagger}(\mathbf{S})^{\mathrm{DFT+D}}_{\mathrm{final\ estimate}}$	127.3	227.7	136.7	151.2	107.5	195.5

[a] Zero-point vibrational energies and thermal contributions to enthalpy barriers are also included. Energies are reported in kJ/mol. [b] Difference between CCSD(T) and RI-MP2 energy barriers on a 3T cluster. [c] For 18T cluster. [d] Contribution to enthalpy at 653 K ($E_0^{\ddagger}(\mathbf{S})_{\mathrm{PBE}}$ is the ZPVE-corrected energy barrier).

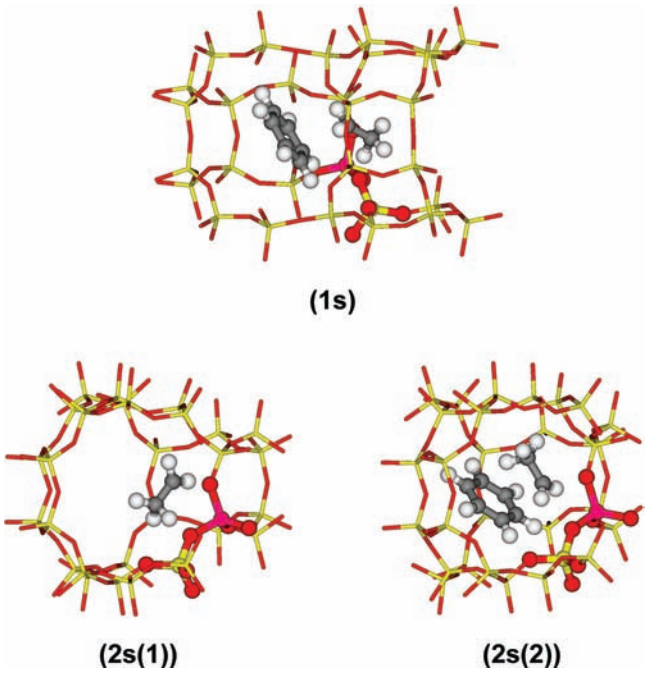

Figure 7. Transition-state structures for one-step and two-step alkylations.

they have not converged and in most cases differ substantially from the periodic limit (see Figure 8b). If the difference between the MP2 and PBE apparent energy barriers is plotted, decaying curves are obtained that converge asymptotically and can be fitted to the analytical expression given in eq 6 (see Figure 9).

The high-level corrections for the intrinsic energy barriers have been obtained by taking the difference between the high-level corrections for the apparent energy barriers and the high-level corrections of the corresponding adsorbate complexes. These energies are listed in the second row of Table 3. The PBE intrinsic barriers for the one-step scheme and for the first step of the two-step scheme are substantially increased by the high-level corrections. For the second barrier of the two-step scheme the high-level correction is significantly smaller.

3.2.3. Extrapolation to Complete Basis Set Limit. The complete basis set limit correction for each intrinsic energy barrier has been determined as the difference between the CBS-limit correction for the apparent energy barrier and the CBS-limit correction for the formation of the corresponding adsorption complex. Depending on the reaction channel, different fragmentations of the system have been used in the counterpoise calculation (see section S.3 of the Supporting Information for details). The CBS limit corrections for the intrinsic energies barrier are listed in the third row of Table 3.

3.2.4. CCSD(T) Corrections. CCSD(T) corrections are listed in the fourth row of Table 3. For the forward reaction steps the differences between CCSD(T) and MP2 are very small (+0.5, −1.9, and −1.0 kJ/mol) showing that MP2 yields energy barriers of CCSD(T) quality. For the reverse reactions larger CCSD(T) corrections are obtained (−12.8, −4.7, and −11.0 kJ/mol) which

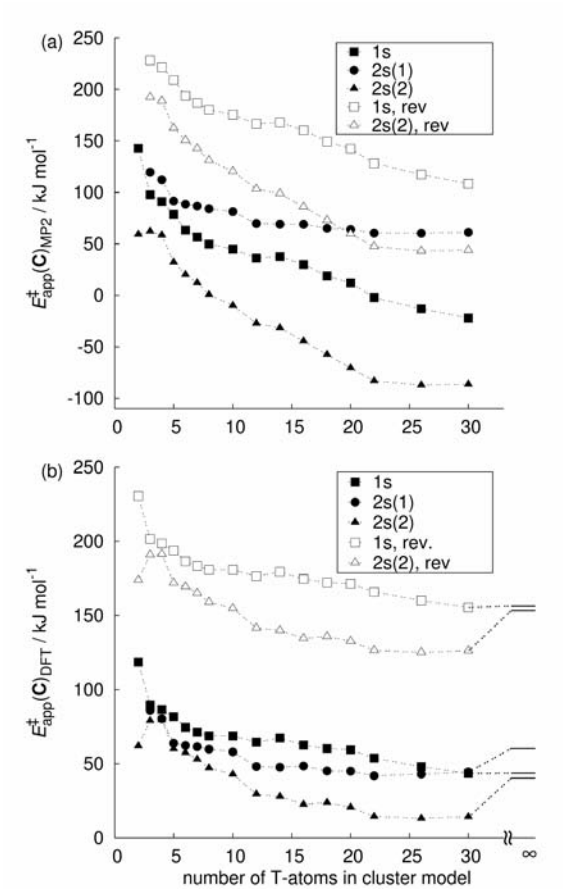

Figure 8. Apparent energy barriers for the one- and two-step alkylations obtained from single-point energy calculations on cluster models of increasing size. (a) MP2/TZVP(P) results. (b) DFT (PBE/QZVP) results. The periodic model limit is included for comparison.

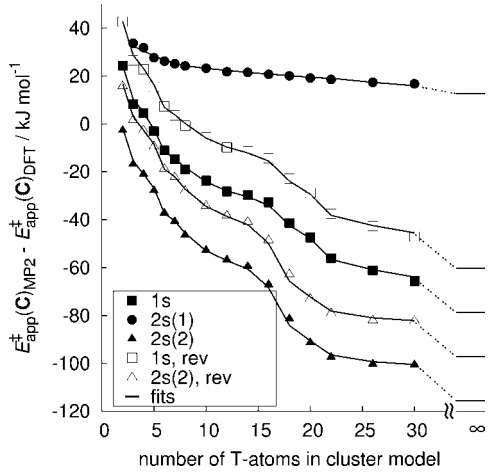

Figure 9. Differences between the two series of apparent energy barriers shown in Figure 8 and extrapolation to the periodic limit.

indicate an overstabilization of the reaction product, adsorbed ethylbenzene, by MP2.

3.2.5. Final Estimate for Energy Barriers. Table 3 shows the final estimate for intrinsic energy barriers which are obtained from the PBE energy barrier, the high-level corrections extrapolated to the periodic limit, the basis set limit corrections, and the CCSD(T) corrections, see eq 3. For the one-step scheme, the energy barrier is 129.7 kJ/mol. For the two-step scheme we obtained 129.7 kJ/mol for the first step and 102.5 kJ/mol for

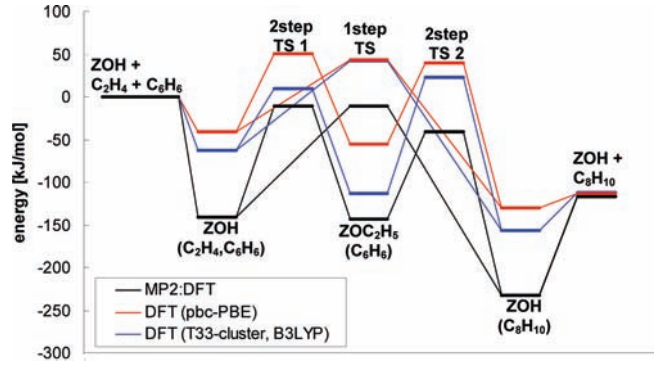

Figure 10. Potential energy profiles for the alkylation of benzene obtained with different methods.

the second step. While the energy barrier for the one-step scheme determined in the present study differs only slightly from that determined in our earlier B3LYP cluster study ($E^{\ddagger}$ = 123.2 kJ/mol)[24] there are significant deviations for the two-step scheme. For the first step the final estimate barrier is 24 kJ/mol higher, while it is 13 kJ/mol lower for the second step. In these calculations of energy barriers for the alkylation, the hybrid MP2:DFT results are affected by the same type of uncertainties as the calculations of adsorption energies. Therefore, an uncertainty range of ±10 kJ/mol is expected.

The *final estimates* of the present study provide a significant improvement in the theoretical description of benzene alkylation over H-ZSM-5, if we keep in mind that the intrinsic barriers from the DFT cluster study strongly depend on the cluster size. This is the result of a partial compensation of two types of errors in plane PBE:[23] missing dispersion which results in too high barriers and self-interaction correction errors which result in systematically too low barriers. Because the former depends much more on the cluster size than the latter, the extent of the compensation and the resulting barriers strongly depend on the cluster size (see also section 3.3).

Figure 10 compares the *final estimate* potential energy profile with the PBE profile and the B3LYP profile for the T33 cluster calculated previously.[24] The *final estimate* profile is shifted down substantially relative to the DFT profiles. More importantly this shift is different for reactants and transition states due to different self-interaction errors.

3.3. DFT+D. 3.3.1. PBE+D//PBE Results. Figures 5 and 6 show the dispersion contributions to the adsorption energies calculated for different cluster sizes according to eq 6 with the transferable parameters of Grimme,[13] (open symbols). The values for the periodic structures (number of T atoms = ∞) are also shown in Table 1 (row 9). Row 10 of Table 1 contains the total PBE+D//PBE adsorption energies (eq 10) which show a substantial improvement compared to plane PBE results. The deviation from the final estimate based on our hybrid MP2:DFT results is small, −6.4, −2.3, +2.7, and +6.6 kJ/mol (−8, −2, +2, and +8%) for **2**, **3**, **4**, and **6**, respectively, i.e. for all physisorption steps except ethene. For ethene physisorption on the silica wall (**7**), on the Brønsted site (**1**), and for ethoxide formation (**5**), PBE+D overestimates the binding energies by 6.5, 12.4, and 26 kJ/mol, in agreement with previous work for isobutene on H-FER.[10,22]

For energy barriers the dispersion contributions and the total PBE+D energies, evaluated as difference between the reactants and the transition structures, are shown in rows 9 and 10 of Table 3. Compared to our *final estimates* for the hybrid MP2:PBE results, the PBE+D barriers, which are affected by the

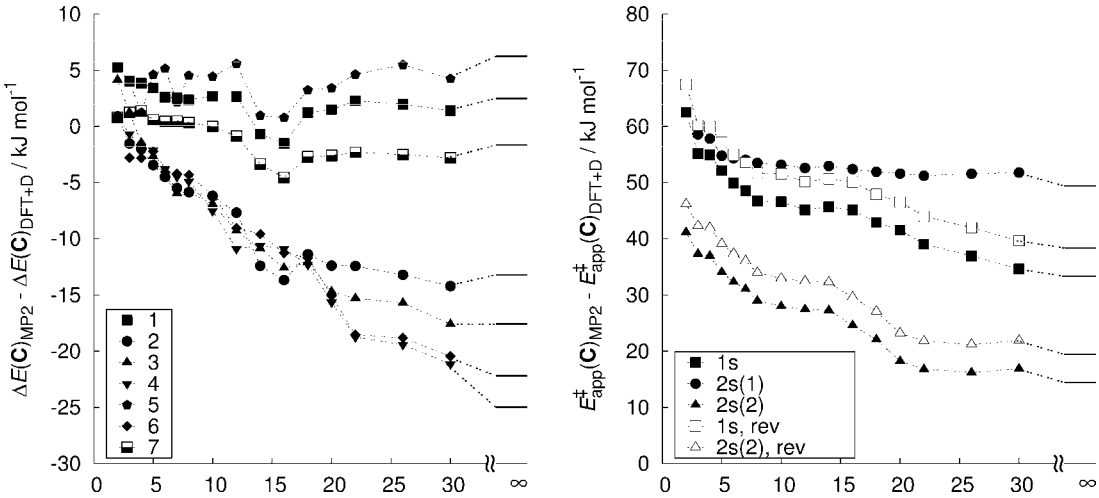

Figure 11. Differences between MP2 and PBE+D results for adsorption energies and apparent energy barriers as function of cluster size.

self-interaction correction error only, are too low by 59.8, 45.6, and 29.3 kJ/mol for **1s**, **2s(1)** and **2s(2)** steps, respectively. This is in the range of 12−62 kJ/mol by which PBE barriers for different types of reactions are known to be too low.[11] The plane PBE barriers are too low by 45.4, 38.1, and 6.6 kJ/mol, respectively, due to partial compensation between missing dispersion (−14.4, −7.5, and −22.7 kJ/mol, row 9 in Table 3) and the self-interaction correction error.

3.3.2. Discussion. In terms of model chemistry the conclusion from this and previous studies[22,23] is that the PBE+D model maintains the performance of the PBE model also in cases for which dispersion is important. That means that PBE+D will show the same underestimation of barriers and the same overstabilization of polar structures as PBE. An improvement would be possible with density functionals that have a smaller self-interaction correction error such as hybrid functionals.

The B3LYP+D model is expected to yield adsorption energies that are close to our hybrid MP2:PBE+ΔCCSD(T) model and to yield improved results for reaction barriers. Reference 11 reports a range of 6−36 for barrier errors with B3LYP compared to 12−62 kJ/mol with PBE. The problem is that calculations with hybrid functionals applying periodic boundary conditions would not be feasible for zeolite catalysts because the unit cells are large and symmetry is low or absent. A possibility is a hybrid B3LYP+D(cluster):PBE+D(pbc) + ΔCCSD(T) scheme, which would maintain the performance of the B3LYP+D model also for extended systems represented by large unit cells and periodic boundary conditions.

The most effective use of PBE+D calculations is probably as low level method in a hybrid scheme. The most expensive part of our hybrid MP2/CBS:PBE scheme is the evaluation of the high-level correction, eq 1, which requires MP2 calculations for different cluster sizes. Figures 5 and 6 show that the dispersion term, calculated with the transferable Grimme parameters, has the same dependency on the cluster size. This means that the high-level correction calculated for PBE+D as the low level method, i.e.

$$\Delta E(\mathbf{C})_{\text{high}}^{\text{DFT+D}} = \Delta E(\mathbf{C})_{\text{MP2}} - \Delta E(\mathbf{C})_{\text{DFT+D}} \qquad (12)$$

depends only weakly on the cluster size in most cases, see Figure 11, which suggests a hybrid MP2/CBS(cluster):DFT+D(pbc) + ΔCCSD(T) approach. Such a scheme would avoid any fitting and the high-level correction would be evaluated for one cluster size $\mathbf{C}_{\text{MP2}}$ only.

$$\Delta E(\mathbf{S})_{\text{final estimate}}^{\text{DFT+D}} = \Delta E(\mathbf{S})_{\text{DFT+D}} + \Delta E(\mathbf{C}_{\text{MP2}})_{\text{high}}^{\text{DFT+D}} + \Delta E(\mathbf{C}_{\text{MP2}})_{\text{MP2}}^{\text{CBS}} + \Delta E(\mathbf{C}_{\text{CC}})_{\text{CCSD(T)}} \qquad (13)$$

Figure 11 suggests that in most cases clusters in the 16T−18T size region would be sufficient. Since MP2/CBS results for T18 have not been calculated for all systems, we use here the T18 results if available and T16 in the other cases to calculate $\Delta E(\mathbf{C})_{\text{high}}^{\text{DFT+D}}$ and $\Delta E(\mathbf{S})_{\text{final estimate}}^{\text{DFT+D}}$ according to eqs 12 and 13. The results for adsorption energies and intrinsic barriers are shown in the bottom rows of Tables 1 and 3, respectively. The deviation from the *final estimate* adsorption energies based on our MP2:DFT results is small for **1**, **2**, **3**, **5** and **7** (−1.2, +1.8, +5.5, −3.0, and −1.0 kJ/mol), i.e. for all steps for which the difference between MP2 and DFT+D adsorption energies does not show large variations beyond the T18 cluster (see Figure 11). Especially the reaction energies for **1**, **5**, and **7,** evaluated with eq 13, deviate significantly less from the MP2:DFT *final estimates* than the PBE+D results, showing that eq 13 offers an attractive approach to improve PBE+D results with reasonable computational costs. The deviation of the intrinsic barriers calculated by means of eq 13 from the *final estimates* is also small (−2.3, +7.0, and +5.9 kJ/mol) for **1s**, **2s(1)** and **2s(2)**, i.e. less than 6%. This remarkable agreement results from error compensation because the MP2-DFT+D results evaluated for the T16 cluster for both reactant states and apparent barriers show similar deviations from the extrapolations to their periodic limits.

3.4. Rate Coefficients for Elementary Steps and Comparison with Experimental Data. Enthalpy barriers are obtained from our *final estimate* energy barriers by adding the zero-point vibrational energies and thermal corrections (rows 7 and 8 in Table 3, respectively), both calculated from PBE frequencies. The intrinsic energy and enthalpy barriers have to be converted into apparent activation energies before they can be compared to experimental data.

Rate coefficients for all elementary reaction steps were calculated according to eq 11. As is justified in section S.5 of the Supporting Information, the partition functions of reactant and transition state were evaluated from vibrational contributions only. For the one-step mechanism the reaction path symmetry

Table 4. Intrinsic Rate Coefficients for the One-Step and Two-Step Mechanisms

reaction	constant	T (K) 603	653	703
$HOZ(C_2H_4 + C_6H_6) \rightarrow HOZ(C_8H_{10})$ (**1s**)	k_1, s^{-1}	5.04×10^0	3.28×10^0	1.64×10^2
	k_{-1}, s^{-1}	3.85×10^{-6}	9.68×10^{-5}	1.54×10^{-3}
$HOZ(C_2H_4) \rightarrow C_2H_5OZ$ (**2s(1)**)	k_1, s^{-1}	8.87×10^0	5.91×10^1	3.00×10^2
	k_{-1}, s^{-1}	4.92×10^2	3.81×10^3	2.22×10^4
$C_2H_5OZ(C_6H_6) \rightarrow HOZ(C_8H_{10})$ (**2s(2)**)	k_1, s^{-1}	2.85×10^4	1.29×10^5	4.75×10^5
	k_{-1}, s^{-1}	4.40×10^{-5}	7.65×10^{-4}	8.89×10^{-3}

Table 5. Preexponential Factors of Elementary Steps in s^{-1}

reaction		T (K) 603	653	703
$HOZ(C_2H_4 + C_6H_6) \rightarrow HOZ(C_8H_{10})$ (**1s**)	ref 24	2.60×10^{10}	2.46×10^{10}	2.35×10^{10}
	this work	2.78×10^{10}	2.68×10^{10}	2.60×10^{10}
$HOZ(C_2H_4) \rightarrow C_2H_5OZ$ (**2s(1)**)	ref 24	1.11×10^{11}	1.07×10^{11}	1.03×10^{11}
	this work	4.75×10^{11}	4.53×10^{11}	4.34×10^{11}
$C_2H_5OZ(C_6H_6) \rightarrow HOZ(C_8H_{10})$ (**2s(2)**)	ref 24	1.41×10^{12}	1.47×10^{12}	1.53×10^{12}
	this work	1.33×10^{12}	1.36×10^{12}	1.39×10^{12}

number was set to $\sigma = 12$ in order to account for the fact that each of the two C-atoms of ethene can react with each of the six C-atoms of benzene. The rate coefficient is therefore larger by a factor of 12 compared to the single-event rate coefficient obtained if all C-atoms were distinguishable. For the first step of the two-step mechanism we used $\sigma = 2$, while for the second step $\sigma = 6$ was employed. The rate coefficients obtained are listed in Table 4 for relevant reaction temperatures. It should be noted that the preexponential factors determined in the present work are similar to those obtained in our cluster study[24] (see Table 5). The largest deviation is observed for the ethoxide formation. For this process the preexponential factor obtained in the present work is higher by a factor of 4 compared to the value obtained in our cluster study. The changes in the rate coefficients compared to those in our cluster study are therefore mostly due to the differences in the calculation of intrinsic energy barriers as well as the consideration of reaction path symmetry numbers.

Experimentally determined rate data for the alkylation of benzene depend on a number of items in addition to the intrinsic rate coefficients. These are in particular the external conditions such as pressure, temperature, and gas-phase composition but also the particle size and shape. All of these factors determine the average concentration of precursor states inside the zeolite channel system and consequently the effective rate of reaction via

$$r = k_1\langle N_{\mathrm{pre},1}\rangle - k_{-1}\langle N_{\mathrm{pre},-1}\rangle \qquad (14)$$

In this equation, r denotes the overall rate of reaction in mol kg^{-1} s^{-1}, k_i are the intrinsic rate coefficients for forward and reverse reactions, and $\langle N_{\mathrm{pre},i}\rangle$ are the average concentrations of precursors for forward and reverse reactions, respectively, in mol kg^{-1}. In a previous publication[27] we have introduced a phenomenological model that relates the external conditions (temperature, pressure, and gas phase composition) to the concentration of precursor states based on the multicomponent adsorption behavior of the ethene−benzene−ethylbenzene mixture as well as on the distribution of these species inside the zeolite channel system. As a result, the rates calculated by means of eq 14 can be compared to experimental data. Alternatively we can use turnover frequencies obtained from

$$\mathrm{TOF} = r/c_{\mathrm{H+}} \qquad (15)$$

where r is the rate of reaction according to eq 14 and $c_{\mathrm{H+}}$ is the concentration of acid sites in mol kg^{-1}, respectively. From calculated turnover frequencies at different temperatures we can obtain the apparent activation energy by means of an Arrhenius plot. Figure 12 shows simulated Arrhenius plots at 2.5 bar overall gas pressure, and a fixed benzene to ethene ratio of 5:1. For the one-step scheme the average concentrations $\langle N_{\mathrm{pre},1}\rangle$ in eq 14 at 603 and 653 K are 1.73×10^{-3} and 7.31×10^{-4} molecules per unit cell, respectively.[27] Note that $\langle N_{\mathrm{pre},-1}\rangle$ was essentially equal to zero in the calculations, as virtually no ethylbenzene was present in the gas phase. Some experimental points[74] are also included in Figure 12. They were determined in a mesoporous and a conventional ZSM-5 sample, respectively. The difference in the activity among the two samples was attributed to diffusional limitation in the case of the

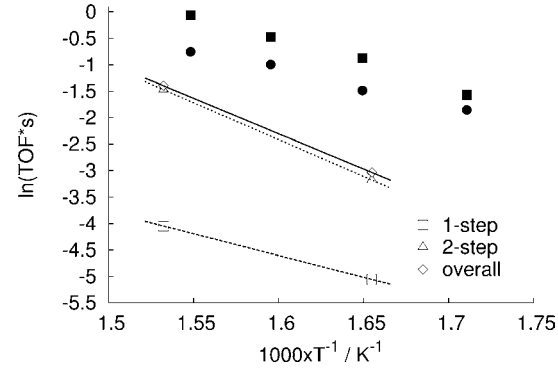

Figure 12. Experimental and simulated Arrhenius plots for the alkylation of benzene at 2.5 bar and a benzene to ethene ratio in the gas phase of 5:1. The experimental data were obtained for mesoporous (■) and conventional (●) H-ZSM-5.[74] The simulated turnover frequencies are plotted for the one-step mechanism, the two-step mechanism, and for the sum of both.

Table 6. Comparison of Apparent Arrhenius Parameters Obtained from *Final Estimates* with Experiments (in kJ/mol and 1/s)

	calcd		obsd	
	E_{app}	A_{app}	E_{app}	A_{app}
1s	66.1	3.41×10^3	58−	2.44×10^4−
2s	112.0	2.09×10^8	76	1.38×10^6
total	107.5	9.74×10^7		

conventional zeolite sample. It should be noted, though, that differences in the multicomponent adsorption equilibrium between the two samples might contribute to the observed differences in activities in addition to the effects of intraparticle diffusion. Therefore, the experimental points shown in Figure 12 define a range of possible turnover frequencies for benzene alkylation over H-ZSM-5 samples. The simulated curves for the one- and two-step schemes both underestimate the experimental data. An overall turnover frequency obtained from the summation of the two contributions[75] is also included in Figure 12. The positions of the simulated Arrhenius plots depend on three factors which are the following: first, our *final estimates* for the intrinsic energy barriers; second, our estimates of the intrinsic preexponential factors; and third, the estimation of precursor concentrations by means of our phenomenological model.[27] Table 6 compares apparent Arrhenius parameters calculated from our *final estimates* with Arrhenius parameters determined from experimental data. The calculated apparent activation energies of the two reaction mechanisms, 66.1 and 112.0 kJ/mol differ substantially. Only the apparent activation energy of the one-step scheme agrees with the experimental data within the uncertainty limit of our calculations. While this could lead to the conclusion that our results for the two-step scheme are not correct, it has to be kept in mind that the energy barrier for the two-step scheme was calculated assuming that ethene enters an empty intersection. This assumption, though, is not correct since an excess of benzene was used in the experiments reported in ref 74. As a result, the probability of ethene finding an unoccupied intersection is lowered considerably because benzene adsorbs much more strongly than ethene in the channel intersection. Therefore, it is likely that under such conditions the two-step mechanism is much less relevant than the one-step scheme because any protonated ethene would react with benzene directly instead of forming a surface ethoxide. Therefore, we limit the comparison with experiments to the one-step mechanism. Under the conditions of a significant excess of benzene in the gas phase the apparent activation energy can also be estimated directly (i.e., without using our continuum model[27]) from our calculated adsorption energies and energy barriers reported in Tables 1 and 3. Then the reaction can be assumed to be intrinsic with respect to benzene but apparent with respect to ethene. As a result we can add the difference of the adsorption enthalpies for reaction **4** and **2** at 653 K (−120.5 and −72.2 kJ/mol) to the intrinsic enthalpy barrier at 653 K (117.2 kJ/mol) to obtain the apparent enthalpy barrier (69.0 kJ/mol). The apparent activation energy is then obtained after adding *RT*. The result, 74.4 kJ/mol, is in reasonable agreement with the value obtained from the continuum model. The difference of 8 kJ/mol indicates the importance of an accurate calculation of the precursor concentration.

One reason for underestimation of the experimental turnover numbers might be connected with uncertainties in the estimation of precursor concentrations. An error range is hard to quantify because reliable high temperature adsorption data are not available to test whether force fields parametrized at ambient temperature are still valid at reaction temperature. Moreover it has been shown that adsorption can be very sensitive to small deviations in the crystal structure of the zeolite under study, especially at low pressures.[76] However, taking into account the results of the latter study, it is unlikely that the uncertainties included in the estimation of the precursor concentration are responsible for the 1 order of magnitude deviation. The second reason is most likely connected to the calculation of intrinsic preexponential factors by means of the harmonic approximation which faces its limits at temperatures as high as needed for hydrocarbon reactions in zeolites. These limitations can be overcome by taking into account entropy effects beyond the harmonic approximation, for example by means of transition path sampling.[77] Finally it should be noted that the experimental data are also subject to uncertainties, the estimation of which is beyond the scope of the present study.

4. Conclusion

A hybrid MP2:DFT + ΔCCSD(T) approach was used to study elementary adsorption and reaction steps involved in the alkylation of benzene with ethene over H-ZSM-5. The dispersion energy contributes substantially to the *final estimates* for the adsorption energies, leading to a reversal of the stability sequence predicted by plane-wave PBE calculations for the adsorption of ethene, benzene, and ethylbenzene on the Brønsted acid site. Calculated adsorption enthalpies are more negative than experimental data by 2−4 kJ/mol per CH_n unit.

The *final estimates* for intrinsic energy barriers deviate significantly from the plane-wave PBE barriers which are systematically too low. Intrinsic energy barriers are converted to apparent activation energies by means of a phenomenological model based on the multicomponent adsorption equilibrium of the ethene−benzene−ethylbenzene mixture.[27] Whereas the two-step mechanism is unlikely to occur under the conditions of the experiment, the apparent activation energy for the one-step alkylation (66 kJ/mol) agrees with the experimental data (58−76 kJ/mol) within the uncertainty limit of our calculations (±10 kJ/mol). Comparison with the intrinsic barrier (129.7 kJ/mol) shows that under the experimental conditions the reaction is essentially intrinsic with respect to benzene, but apparent with respect to ethene. The calculated turnover frequencies are underestimated compared to the experimental values which is most likely due to the harmonic approximation applied in the calculation of preexponentials. Future improvements require sampling the anharmonic potential energy surface. Part of the remaining deviations for both barriers and preexponentials can be ascribed to the fact that our calculations refer to one particular site in the zeolite in contrast to experimental data that are averages over a distribution of sites.

As far as methods are concerned, we have shown in this and in previous studies[9,21−23] that a reliable description of hydrocarbon reactions in zeolites, in particular, and reactions occurring on a local site in a large chemical system, in general, is only

(74) Christensen, C. H.; Johannsen, K.; Schmidt, I.; Christensen, C. H. *J. Am. Chem. Soc.* **2003**, *125*, 13370–13371.
(75) Laidler, K. J. *Chemical Kinetics*, 3rd. ed.; Harper & Row: New York, 1987.
(76) Zimmermann, N. E. R.; Haranczyk, M.; Sharma, M.; Liu, B.; Smit, B.; Keil, F. J. *Mol. Simul.*, submitted.
(77) Bučko, T.; Benco, L.; Dubay, O.; Dellago, C.; Hafner, J. *J. Chem. Phys.* **2009**, *131*, 214508–1/11.

possible with a method that includes dispersion, limits the self-interaction correction error, and takes long-range electrostatic effects into account. The majority of routine DFT calculations currently performed and published in these areas do not meet these requirements and are therefore affected by uncontrolled and sizable errors. In contrast, our hybrid MP2:DFT + ΔCCSD(T) method meets all these requirements. In the context of model chemistry it is a way to maintain the performance of the MP2/CBS+ΔCCSD(T) model established for molecules also for extended systems represented by large unit cells and periodic boundary conditions. The method is by no means limited to hydrocarbon reactions in zeolites but is generally applicable to large chemical systems in which dispersion interactions play a role and/or self-interaction correction errors change along the reaction coordinate. Typical examples are adsorption of molecules on, and reactions with, different types of surfaces such as oxides, semiconductors, graphite and carbon nanotubes, or biopolymers. It has been successfully used to calculate isotherms for hydrogen adsorption in metal−organic frameworks,[78] and work on hydrocarbon adsorption on oxide surfaces is in progress.[79] Another area of application is solvation in which an increasing number of solvent molecules is included in the cluster.

Application of our hybrid approach is not bound to the use of specific codes for the high-level (MP2) and low-level (periodic DFT) method, and when used with fixed geometric structures that have been obtained at the low level as done here, it does not even require a program that links the codes. Nevertheless, its general use may be hampered by the large number of demanding MP2 calculations to be performed and the need to fit the difference between the MP2 and DFT results (high-level correction). However, this we did only to generate benchmark data for simpler protocols such as the hybrid MP2(cluster):DFT+D(pbc) approach discussed in section 3.3.2. The latter needs a DFT code with some means of including dispersion and periodic boundary conditions. A stand-alone implementation of the Grimme term that can be combined with periodic DFT codes is freely available.[10] This DFT+D code is used to optimize a structure. For the structure obtained, a cluster model needs to be defined on which MP2 single-point calculations are performed by any MP2 code available. Special QM:QM coupling software with periodic boundary conditions[80] is available from two laboratories[10,21,81,82] but is only needed if there is a reason to improve the DFT+D structures and to optimize on the hybrid MP2(cluster):DFT+D(pbc) potential energy surface.

Acknowledgment. The present work was supported by the Deutsche Forschungsgemeinschaft (DFG) in priority program SPP 1155 and the Methane Conversion Cooperative supported by BP. Computations were partly carried out at the Norddeutscher Verbund für Hoch- und Höchstleistungsrechnen (HLRN). N.H. acknowledges Tomáš Bučko for providing an implementation of the improved dimer method into VASP.

Supporting Information Available: Possible location of acidic site in H-ZSM-5; description of procedure for extrapolation to the complete basis set limit and details of BSSE calculations for transition states and intermediates; discussion of different approaches to calculate the reactant partition function; influence of unit cell parameters on PBE energies; additional data illustrating the cluster size dependence of adsorption energies and energy barriers; fit parameters; energies and Cartesian coordinates of stationary points; complete refs 55 and 82. This material is available free of charge via the Internet at http://pubs.acs.org.

JA102261M

(78) Sillar, K.; Hofmann, A.; Sauer, J. *J. Am. Chem. Soc.* **2009**, *131*, 4143–4150.
(79) Tosoni, S.; Sauer, J. Manuscript in preparation.
(80) Sauer, J.; Sierka, M. *J. Comput. Chem.* **2000**, *21*, 1470–1493.
(81) Sierka, M.; Sauer, J. *J. Chem. Phys.* **2000**, *112*, 6983–6996.
(82) Sherwood, P.; et al. *J. Mol. Struct. (THEOCHEM)* **2003**, *632*, 1–28.